ACS Macro Letters

pubs.acs.org/macroletters Letter

Polyelectrolyte–Carbon Dot Complex Coacervation

Pankaj Kumar Pandey,* Arvind Sathyavageeswaran, Nickolas Holmlund, and Sarah L. Perry*

Cite This: ACS Macro Lett. 2025, 14, 43–50 Read Online

ACCESS | Metrics & More | Article Recommendations | Supporting Information

ABSTRACT: This Letter presents complex coacervation between the biopolymer diethylaminoethyl dextran hydrochloride (DEAE-Dex) and carbon dots. The formation of these coacervates was dependent on both DEAE-Dex concentration and solution ionic strength. Fluorescence spectroscopy revealed that the blue fluorescence of the carbon dots was unaffected by coacervation. Additionally, microrheological studies were conducted to determine the viscosity of these coacervates. These complex coacervates, formed through the interaction of nanoparticles and polyelectrolytes, hold a promising role for future applications where the combination of optical properties from the carbon dots and encapsulation via coacervation can be leveraged.

In the domain of materials science, significant progress has been made in the field of nanoscience and soft matter. Researchers seek to explore new self-assembled architectures based on polymers and nanoparticles to explore new optoelectronic and biomedical applications.[1,2] Complex coacervation is an example of self-assembly between two oppositely charged polymers, resulting in a unique associative liquid–liquid phase separation that results in a polymer-rich coacervate coexisting with a polymer-poor supernatant.[3,4] Coacervation depends on the pH and ionic strength.[5,6] The impact of salt ions on coacervation arises from the critical entopic reliance on the release of counterions. High salt concentration decreases the entropic driving force that facilitates complex formation, thereby destabilizing liquid–liquid phase separation. Coacervates represent a fascinating avenue of research with promising applications across multiple fields like drug delivery and tissue engineering.[7,8]

Polymers can self-assemble with nanoparticles, forming higher-order structures including solids such as nanocomposites colloidal crystals, or nanopolymer composites with multifunctional properties and applications,[9−13] but it has been less common to form liquid materials like coacervates. Yu et al. explained the theoretical mechanism of how nanoparticles could interact with polymers to form coacervates,[14] though they did not have supporting experimental results at that time. Experimentally, work by Gaash et al., demonstrated the potential for liquid–liquid phase separation involving peptide-based coacervates in the presence of nanoparticle-like carbon dots.[15] Here, the use of carbon dots is particularly intriguing because of their tunable size and surface chemistry,[16−18] as well as their ability to support coacervation.[19−29]

Carbon dots are a unique type of nanoparticle due to their low toxicity, high photoluminescence, good biodegradability, and water solubility.[19−27] Carbon dots can be derived from biological sources and do not require the use of toxic solvents and chemicals.[30−35] Furthermore, this biocompatibility can be leveraged alongside their intrinsic fluorescence to allow for biosensing applications.[15,34−37] The surfaces of carbon dots can be easily functionalized and have a large surface area, providing active sites for enhanced electrochemical activity.[36] For instance, Chen et al., showed that carbon dots can increase the conductivity of hybrid materials.[37] Additionally, integrating carbon dots into coacervate structures has the potential to improve previously designed energy storage solutions.[38] A coacervate matrix could also prevent carbon dots from aggregation, thereby eliminating the common problem of nanoparticle quenching and ensuring that the optical and functional properties of the carbon dots are preserved.[28,29] Combining carbon dots with coacervates also has the potential to facilitate responsive fluorescent materials that can be prepared entirely in an aqueous milieu while also leveraging the ability for coacervates to encapsulate drugs or other molecules,[14,15,39−43] including proteins or other biomolecules that denature in organic solvents. This combination of features could allow for tandem therapeutic delivery with nanoparticles for imaging for theranostic approaches,[28,44] as well as improved therapeutic effectiveness and reduced side effects.[30−38]

To date, studies looking into complex coacervation between carbon dots and polyelectrolytes are still in the early stages,[28,29,44] with only a single system having been described (*i.e.*, carbon dots in complex with poly(diallyldimethylammonium), PDADMA). The biocompatible and biobased aspects of carbon dots can be further leveraged in materials via complexation with biopolymers. In this work, we

Received: November 9, 2024
Revised: December 10, 2024
Accepted: December 16, 2024
Published: December 19, 2024

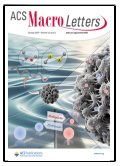

https://doi.org/10.1021/acsmacrolett.4c00745
ACS Macro Lett. 2025, 14, 43–50

have explored the complex coacervation between the cationic biopolymer diethylaminoethyl dextran hydrochloride (DEAE-Dex) and anionic carbon dots. This coacervation can be tuned in response to physiochemical parameters, enabling stimuli-responsiveness and tunability at a range of conditions that is relevant to physiological conditions.[45,46] Furthermore, while previous studies focused on dispersions of coacervate nanodroplets which are useful for delivery[28,44] and as nanoreactors,[29] our efforts look to characterize the coacervate material itself, including its rheological properties. This work represents a new aspect of complex coacervation involving a biopolymer and nanoparticles, and potentially paves the way for novel research avenues in future applications.

Materials: Diethylaminoethyl dextran hydrochloride (DEAE-Dex) was purchased from Sigma-Aldrich as a solid powder. Urea (M_w = 60.06 g/mol), citric acid monohydrate (M_w = 210.14 g/mol), sodium chloride (NaCl), hydrochloric acid (HCl), sodium hydroxide (NaOH) and carboxylate-modified microspheres (Red FluoSpheres, 500 nm) were all purchased from Thermo Fisher Scientific. Deionized water was obtained from a Milli-Q water purification system (Millipore Sigma Advantage A10) at a resistivity of 18.2 MΩ.

Stock solutions: A stock solution of DEAE-Dex was prepared gravimetrically (pH = 3.8) at a concentration of 2% (w/v) by mixing in Milli-Q water at 25 °C with continuous stirring for 12 h. Urea and citric acid stock solutions were similarly prepared at 800 mM and 250 mM concentrations (pH = 4). NaCl stock solution was prepared at 2 M. 1 M HCl and 1 M NaOH stock solutions were used to adjust pH whenever necessary. The carbon dot stock solution was prepared at 0.6% (w/v).

Synthesis of carbon dots: The carbon dots were synthesized using a method similar to literature reports.[47] The stock solutions of urea and citric acid were mixed in a 3:1 molar ratio with a total volume of 20 mL and placed in a 50 mL polytetrafluoroethylene-lined hydrothermal vessel, which was then placed in an oven (Oakton) at 180 °C for 4 h. After 4 h, the vial was allowed to cool down to room temperature in air. Then, the mixture was transferred to a 1 kDa cutoff dialysis bag (Spectrum Laboratories) and placed in a 1 L Milli-Q water bath for purification. The dialysis was conducted for a total duration of 24 h, with the water changed every 4 h. The carbon dot suspension obtained after purification was freeze-dried (Labconco FreeZone 2.5 Plus) into a powder, which was later dissolved to make stock solutions.

Preparation of carbon dot coacervates: All coacervate samples were prepared by sequentially adding Milli-Q water, followed by salt (if necessary), carbon dots, and then DEAE-Dex, with thorough mixing between each addition. For stoichiometry experiments, the relative amounts of DEAE-Dex and carbon dot were varied to identify the ratio at which maximum turbidity occurred. This involved adding increasing amounts of DEAE-Dex while maintaining a constant amount of carbon dots in the samples. In our stoichiometry experiments, we define the DEAE-Dex weight fraction as following:

$$\text{DEAE-Dex wt. fraction} = \frac{[\text{DEAE-Dex}]}{[\text{DEAE-Dex}] + [\text{carbon dot}]}$$

The composition where maximum turbidity was observed was taken to be the optimum condition for coacervate formation and was used in all subsequent experiments. Samples at the optimum composition were then prepared with increasing concentration of NaCl to identify the salt resistance, or the point at which phase separation was no longer observed. This transition was determined using a combination of turbidity and optical microscopy.

Turbidimetry: Turbidity was used to estimate the extent of phase separation as a function of charge stoichiometry and salt concentration. Turbidity tests were conducted using a microplate reader (BioTek Synergy H1). Turbidity was measured at 562 nm and 25 °C and subtracted from the baseline with water. Samples for turbidity measurements (i.e., stoichiometry and salt resistance experiments) were prepared at a 120 μL scale and pipetted in triplicate into a 384-well plate (Fisher) immediately after sample preparation. Triplicate measurements were made for each sample, and all experiments were repeated three times. Turbidity data are graphed as the average of these replicates. Error bars represent the calculated standard deviation.

Transmission electron microscopy (TEM): The carbon dots samples for TEM were prepared in water at 0.02% (w/v) and sonicated in a bath sonicator (BRANSONIC CPX2800H) for 3 h. Then, the sample was drop-cast onto a carbon-coated copper grid (Ted Pella Inc.) for TEM imaging. The particle size distribution was determined using a JEOL-JEM-2200FS Energy Filtered Transmission Electron Microscope (JEOL USA), and elemental composition in the sample was determined using an Oxford X-MAX 80 mm^2 Energy-dispersive X-ray spectrometer (EDS). The size of particles observed via TEM was determined using ImageJ[48−50] using 41 particles.

Zeta potential: A Malvern Zetasizer ZSP was used to perform zeta potential measurements. Each measurement included 11 scans and all measurements were repeated three times. The coacervate samples for zeta potential measurements were prepared at a 100-fold dilution compared to the samples used in the stoichiometry experiments.

UV−vis spectroscopy: A SpectraMax iD3 microplate reader from Molecular Devices was used for UV−vis and fluorescence spectroscopy measurements. A 96-well black plate from Corning Costar was used.

Optical and fluorescence microscopy: Visual inspection of coacervates was performed in brightfield and fluorescence mode using a Zeiss Axio Observer Z1 inverted fluorescence microscope with an Orca R2 camera and a 20× objective. Imaging was performed immediately after the turbidity measurement on the same samples in the well plate. For fluorescence imaging, a DAPI filter was used. The fluorescence microscopy was done at a 10-fold dilution compared to the samples used in the stoichiometry experiments.

Microrheology: Microrheology was performed via fluorescence microscopy using samples prepared on glass slides sandwiched with a coverslip (1.0 cm × 0.5 cm) using double sided tape. A 120 μL sample was prepared at the condition where maximum turbidity was observed in the stoichiometry experiment. More specifically, the sample was prepared at a 0.33 DEAE-Dex weight fraction (*i.e.*, a final concentration of 0.003% (w/v) DEAE-Dex and 0.006% (w/v) carbon dot). A 120 μL sample was prepared initially in a 1 mL microcentrifuge tube, vortexed, and then split into three separate aliquots of 40 μL each. Fluorescent microspheres (2.16×10^{-5} % (w/v)) were then added to the sample and vortexed so that the microspheres were encapsulated inside the coacervate droplets. No centrifugation was performed to avoid the precipitation of the beads. 30 μL of the sample was then pipetted into an

https://doi.org/10.1021/acsmacrolett.4c00745
ACS Macro Lett. 2025, 14, 43−50

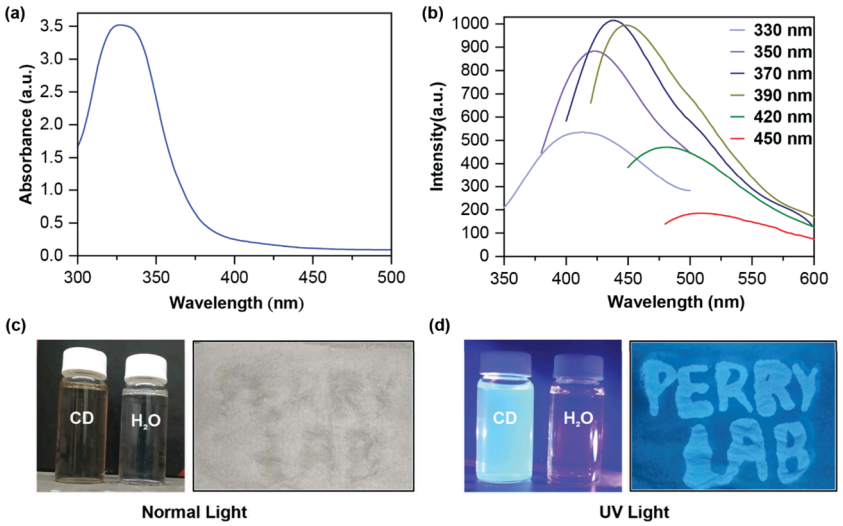

Figure 1. (a) UV absorbance spectrum for a suspension of carbon dots in water. (b) Fluorescence emission spectra of carbon dots at different excitation wavelengths. Photograph of a suspension of carbon dots in water alongside a vial of water, and the carbon dot solution painted onto paper in (c) normal light and (d) when exposed to UV light.

imaging chamber created by sandwiching a glass slide and a coverslip. The chamber was sealed with Loctite epoxy to avoid leakage of the sample. The sample was allowed to equilibrate for 1 h to allow the coacervate droplets to coalesce. Finally, the motion of the fluorescent beads was recorded using a DsRed filter at 5 frames per second (fps) using a 40× objective with a 50 ms exposure time. The resulting images were then analyzed to obtain the mean-squared displacement (MSD) as a function of lag time. Data analysis was performed in MATLAB. For more information see the Supporting Information.

In this study, our primary objective was to investigate the complex coacervation between carbon dots and the cationic biopolymer DEAE-Dex. Anionic carbon dots were synthesized using the hydrothermal method with urea and citric acid as the starting materials.[51,52] Before studying coacervation, we first characterized the resulting carbon dots,[53,54] including their optical and morphological properties.

Figure 1a shows the UV−visible spectrum of carbon dots with an excitation absorption edge wavelength around 350 nm. The fluorescence spectrum exhibited a prominent emission peak at 450 nm (Figure 1b), when excited around 370 nm, as expected for carbon dots.[55] The emission properties of the carbon dots were found to be dependent on excitation wavelength, with a red-shifted emission peak observed as excitation varied from 330 to 450 nm. This phenomenon is characteristic of carbon nanoparticles derived from natural sources and is attributed to the presence of different emissive sites on the carbon dot surfaces.[51] Upon irradiation at 330 to 450 nm, we observed the emission of a strong blue light from the light-green carbon dot aqueous solution (Figure 1c,d).

To characterize the size of our carbon dots, we performed transmission electron microscopy (TEM). Figure 2a shows a TEM micrograph of the as-synthesized carbon dots, highlighting their various sizes and shapes. High-resolution imaging allows for visualization of the characteristic *d*-spacing of approximately 1.9 Å, which is close to the reported *d*-spacing for the 100 facet of graphitic carbon.[52,56] Analysis of particle size revealed an average diameter of 8.94 ± 0.13 nm, consistent with a Gaussian distribution model (Figure 2b). Our findings agree well with previous literature reports of carbon dots dispersed in water.[53,57,58]

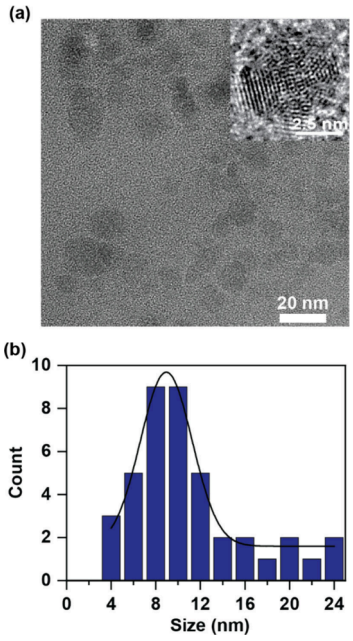

Figure 2. (a) TEM image of carbon dots. The inset shows the interplanar spacing within the carbon dot and (b) the corresponding size histogram for the observed nanoparticles fitted by a Gaussian $y = y_0 + \frac{A}{wC}e^{(-B(x-x_c)^2/w^2)}$ (where y_0 is the baseline of the Gaussian curve, A is an area under the Gaussian curve, B is a constant that determines the peak shape, x_c is the peak center, w is full width at half-maximum (fwhm), the exponential term shows the shape of Gaussian curve, and C is a normalization factor to relate A to the area under the curve).

Complex coacervation between DEAE dextran and carbon dots: Prior reports have reported a negative zeta potential for similar types of carbon dots.[59−61] As complex coacervation involves electrostatic associations between oppositely charged macro-ions, this is an important consideration. Our measurements indicated a zeta potential of −52 mV at pH 4, confirming that our carbon dots could be used as the macro-anion for complex formation with a cationic polymer.

https://doi.org/10.1021/acsmacrolett.4c00745
ACS Macro Lett. 2025, 14, 43−50

To explore the potential for complex coacervation, we combined our anionic carbon dots with the cationic biopolymer DEAE-Dex at pH 4. This acidic solution condition was chosen because it allowed for the amine groups in DEAE-Dex to be fully protonated[62] while also interacting with the negatively charged carbon dots. We used turbidity to examine the effect of the relative amount of DEAE-Dex and the carbon dot on coacervate formation. We observed a maximum in the turbidity signal at a DEAE-Dex weight fraction of 0.33 (Figure 3a). The formation of liquid droplets was also clearly evident via microscopy (Figure 3a, inset).

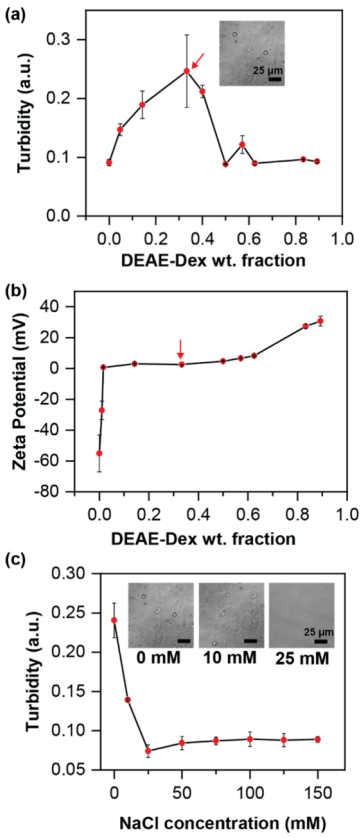

Figure 3. (a) Turbidity as a function of the weight fraction of DEAE-Dex. The inset micrograph shows the formation of liquid droplets. (b) Zeta potential for complex coacervates of DEAE-Dex and carbon dots as a function of increasing weight fraction of DEAE-Dex. (c) Turbidity as a function of increasing NaCl concentration for samples containing a 0.33 weight fraction of DEAE-Dex. The inset micrographs are shown for three different salt concentrations, highlighting the loss of phase separation with increasing salt.

For polymer−polymer coacervates, maximum complexation typically corresponds to conditions of charge neutrality. However, it is difficult to assess the number and concentration of ionizable groups on both the carbon dots and the DEAE-Dex, given their poorly defined structures. Thus, we instead chose to use zeta potential to quantify the charge state of our coacervates. As seen in Figure 3b, as the DEAE-Dex weight fraction increased from 0.00 to 0.02 the overall zeta potential of the mixture approached 0 mV and remained close to 0 mV across a range of compositions centered around a DEAE-Dex weight fraction of 0.33, indicating charge neutralization. Further increases in DEAE-Dex weight fraction led to an excess of positive charge in the mixture. These results are consistent with our observations of turbidity and suggest a correlation between maximum coacervate formation and charge neutrality for this system.

We further examined the effect of salt on coacervation at the optimal weight fraction of 0.33. Figure 3c shows a plot of turbidity as a function of added NaCl concentration. Coacervation was observed in the presence of low concentrations of salt (<25 mM), but further increases in salt decreased the turbidity signal to the point where phase separation was no longer observed via microscopy (Figure 3c, inset). Thus, we identified 25 mM NaCl as the salt resistance. This value of the salt resistance is very low compared to other DEAE-Dex-based coacervates. For example, the salt resistance of DEAE-Dex and DNA was reported to be 0.9 M,[63] while coacervation between DEAE-Dex and pectin has a reported salt resistance 150 mM.[64] These studies suggest a stronger binding interaction between the various polymer−polymer systems compared to polymer-carbon dots. This difference could be a result of potentially fewer charges on the carbon dots and/or a higher solubility of the carbon dots as compared with the other polymers.

Similarly, the salt resistance for our system was low compared to that for carbon dot coacervates made with poly(diallyldimethylammonium) (PDADMA), which had a reported salt resistance around 400 mM NaCl.[28] Here, the difference in stability could be a consequence of the lower charge density of the DEAE-Dex, including the potential for incomplete ionization of the tertiary amines, the hydrophobicity of the PDADMA and/or the presence of other interactions with the surface. These results highlight the need for more studies to elucidate not only the role of charged groups, but also the ways in which other features of the polymer might interact with the carbon dot surface. This knowledge would allow for the design of materials that can respond to very subtle changes in the environment, particularly in the range of physiological conditions for delivery and theranostic applications.

After successfully characterizing coacervate formation and stability, we next studied the fluorescence of the coacervates. We examined the fluorescence spectra of the coacervate, supernatant, and carbon dot solution (Figure 4a). The fluorescence spectrum of the coacervates showed strong intensity compared to the supernatant and the original carbon dot solution. This result confirmed that a significant fraction of the carbon dots participate in coacervate formation. We would note that no shift in the fluorescence was observed upon coacervate formation. Thus, it would seem as though the electrostatic complexation did not affect the electronic states of the carbon dots.[65,66] The bright emission of the coacervates can also be clearly seen in the images in Figure 4b, both with the fluorescent blue droplets and with the brightly glowing dense coacervate phase in the microcentrifuge tube.

The presence of strong fluorescence in our coacervates was particularly exciting as previous reports have described strong quenching due to aggregation when mixed into a polymer medium.[67,68] Indeed, a previous report by Gaash et al., saw decreases in fluorescence intensity over time when carbon dots were encapsulated into a peptide-based condensate that forms via cation-pi interactions.[15] We hypothesize that the charge-driven assembly of coacervates via direct electrostatic interactions with the carbon dots likely helps to mitigate aggregation of particles. Our observations are also consistent

https://doi.org/10.1021/acsmacrolett.4c00745
ACS Macro Lett. 2025, 14, 43−50

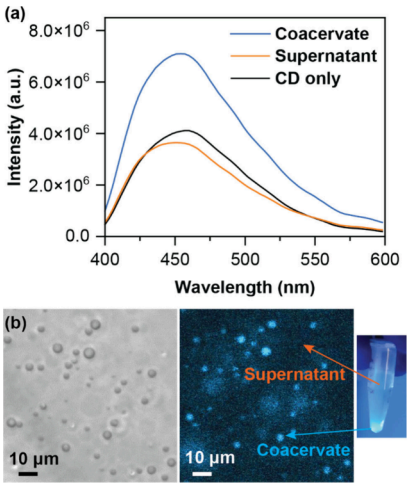

Figure 4. (a) Fluorescence emission spectra for coacervate, supernatant, and a carbon dot solution excited at 370 nm. (b) Brightfield and fluorescent micrographs for DEAE-Dex-carbon dot coacervates, along with a photograph of a microcentrifuge tube containing sedimented, fluorescent coacervates and a weakly emissive supernatant.

with results using PDADMA which showed no loss of fluorescence intensity over the course of a week.[28]

Material properties: Lastly, we investigated the microrheological properties of carbon dot-based coacervates using particle tracking microrheology. We tracked the mean squared displacement (MSD) of fluorescent beads embedded in the coacervate as a function of lag time (Figure S1). In Figure 5, brightfield optical micrographs (Figure 5a), fluorescence micrographs (Figure 5b), and merged images (Figure 5c) show how the samples were visualized and the movement of beads (see inset, Figure 5d).

Figure 5d shows the expected power-law dependence of mean MSD $\propto$ (lag time)$^{\alpha}$, where α is the power-law exponent, the value of which provides insight into the viscous or viscoelastic properties of the material (see SI for more details).[69−71] Our data analysis revealed a power-law exponent of $\alpha = 0.94 \pm 0.03$, indicating that the motion within the coacervates was slightly subdiffusive or very close to the diffusive. Further, a plot of G' and G'' vs frequency (Figure S2a) shows the dominance of the viscous behavior of coacervates in the accessible frequency range, as is typical for many coacervate systems.[69,72] Additionally, the motion of the beads in the coacervate exhibited a Gaussian probability distribution (Figure 5e), suggesting that the particles are experiencing a homogeneous medium relative to the length scale of the particles. The viscosity of the coacervate was shown as a function of frequency (ω) (Figure S2b). The overall viscosity of coacervate was found to be to be 0.93 ± 0.20 Pa·s, which is roughly 1000 times higher than water and is comparable to other coacervate systems.[69,73−76]

Here, we report the complex coacervation of anionic, blue fluorescent carbon dots with the cationic biopolymer DEAE-Dex. The complex coacervate phase maintains the blue fluorescence of the carbon dots without apparent quenching due to particle aggregation. While the stability of these carbon dot coacervates against dissolution by salt was relatively low (~25 mM), a comparison of our results with previous reports[28] suggests that this could be a consequence of relatively low charge density and high solubility of both of our coacervating species, and that the salt stability could be tuned based on the characteristics of the complexing polymer. However, despite these relatively weak interactions, microrheology characterization showed the viscosity of these coacervates to be similar to other coacervate materials, and approximately 1000 times higher than water.

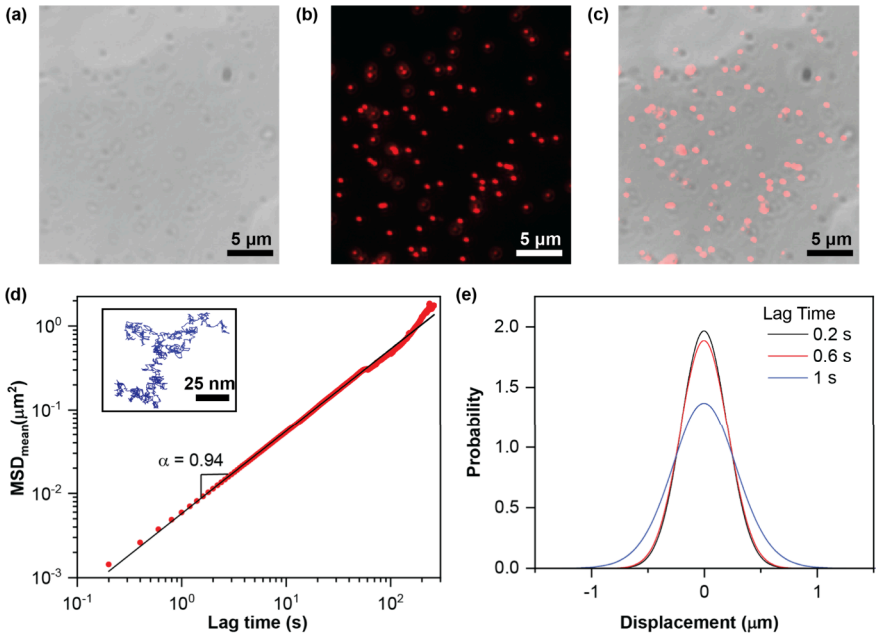

Figure 5. (a) Brightfield optical micrograph, and the corresponding (b) fluorescence micrograph. (c) The merged image demonstrates the incorporation of fluorescent beads into the coacervate. (d) Mean of mean squared displacement (MSD) vs lag time for bead trajectories in coacervates. The dotted line shows the power-law fit. Inset shows an example trace of bead motion in the coacervate. (e) Probability distribution of displacement with time.

https://doi.org/10.1021/acsmacrolett.4c00745
ACS Macro Lett. 2025, 14, 43−50

To date, the small number of reports describing complex coacervation involving carbon dots has been largely limited to applications involving nanodroplet dispersions.[28,29,44] Here, we have characterized a coacervate system that leverages the biopolymer DEAE-Dex, including the rheological aspects of the coacervate. This characterization suggests that carbon dot coacervates could be processed in much the same way as polymer-based coacervates. In addition to the previous demonstrations of carbon dot coacervate dispersions in various bioimaging, theranostic, and catalytic applications,[28,29,44] we propose that carbon dot coacervates could also be used as bulk materials in nonwovens,[77,78] membranes for separations,[79] or other coatings[80,81] where their light-emitting and/or catalytic properties could be leveraged to enhance device performance.

■ ASSOCIATED CONTENT

Supporting Information

The Supporting Information is available free of charge at https://pubs.acs.org/doi/10.1021/acsmacrolett.4c00745.

Figures S1 and S2, Table S1, microrheology algorithm, and parameters for particle detection (PDF)

■ AUTHOR INFORMATION

Corresponding Authors

Sarah L. Perry − *Department of Chemical Engineering, University of Massachusetts Amherst, Amherst, Massachusetts 01003, United States;* orcid.org/0000-0003-2301-6710; Email: perrys@engin.umass.edu

Pankaj Kumar Pandey − *Department of Chemical Engineering, University of Massachusetts Amherst, Amherst, Massachusetts 01003, United States;* orcid.org/0009-0001-2304-5135; Email: pandeypankajjnu@gmail.com

Authors

Arvind Sathyavageeswaran − *Department of Chemical Engineering, University of Massachusetts Amherst, Amherst, Massachusetts 01003, United States*

Nickolas Holmlund − *Department of Chemical Engineering, University of Massachusetts Amherst, Amherst, Massachusetts 01003, United States*

Complete contact information is available at: https://pubs.acs.org/10.1021/acsmacrolett.4c00745

Author Contributions

CRediT: **Pankaj Kumar Pandey** conceptualization, data curation, formal analysis, investigation, methodology, supervision, writing - original draft, writing - review & editing; **Arvind Sathyavageeswaran** formal analysis, investigation, supervision, writing - original draft, writing - review & editing; **Nickolas Holmlund** software; **Sarah L Perry** funding acquisition, supervision, writing - review & editing.

Notes

The authors declare no competing financial interest.

■ ACKNOWLEDGMENTS

The authors acknowledge Dr. Alexander Ribbe for his assistance in collecting the TEM and EDS data in the Electron and Scanning Probe Microscopy Core Facility at the University of Massachusetts Amherst. We are also thankful to Dr. Stephen Eyles for his help with zeta potential measurements in the Biophysical Characterization Facility in the Institute for Applied Life Sciences at the University of Massachusetts Amherst. This work was supported by the National Science Foundation (DMR-1945521) and BASF SE through NORA (North American Research Alliance).

■ REFERENCES

(1) Maity, N.; Ghosh, R.; Nandi, A. K. Optoelectronic Properties of Self-Assembled Nanostructures of Polymer Functionalized Polythiophene and Graphene. *Langmuir* **2018**, *34* (26), 7585−7597.

(2) Zhang, H.; Liu, Y.; Yao, D.; Yang, B. Hybridization of Inorganic Nanoparticles and Polymers to Create Regular and Reversible Self-Assembly Architectures. *Chem. Soc. Rev.* **2012**, *41* (18), 6066−6088.

(3) Yan, Y.; Kizilay, E.; Seeman, D.; Flanagan, S.; Dubin, P. L.; Bovetto, L.; Donato, L.; Schmitt, C. Heteroprotein Complex Coacervation: Bovine β - Lactoglobulin and Lactoferrin. *Langmuir* **2013**, *29*, 15614−15623.

(4) Dubin, P.; Stewart, R. J. Complex Coacervation. *Soft Matter* **2018**, *14* (3), 329−330.

(5) Perry, S. L.; Li, Y.; Priftis, D.; Leon, L.; Tirrell, M. The Effect of Salt on the Complex Coacervation of Vinyl Polyelectrolytes. *Polymers (Basel)* **2014**, *6* (6), 1756−1772.

(6) Priftis, D.; Laugel, N.; Tirrell, M. Thermodynamic Characterization of Polypeptide Complex Coacervation. *Langmuir* **2012**, *28* (45), 15947−15957.

(7) Sümbelli, Y.; Mason, A. F.; van Hest, J. C. M. Toward Artificial Cell-Mediated Tissue Engineering: A New Perspective. *Adv. Biol.* **2023**, *7* (12), No. 2300149.

(8) Margossian, K. O.; Brown, M. U.; Emrick, T.; Muthukumar, M. Coacervation in Polyzwitterion-Polyelectrolyte Systems and Their Potential Applications for Gastrointestinal Drug Delivery Platforms. *Nat. Commun.* **2022**, *13* (1), 2250.

(9) Zhang, L.; Jean, S. R.; Ahmed, S.; Aldridge, P. M.; Li, X.; Fan, F.; Sargent, E. H.; Kelley, S. O. Multifunctional Quantum Dot DNA Hydrogels. *Nat. Commun.* **2017**, *8*, 381.

(10) Pandey, P. K.; Preeti; Rawat, K.; Prasad, T.; Bohidar, H. B. Multifunctional, Fluorescent DNA-Derived Carbon Dots for Biomedical Applications: Bioimaging, Luminescent DNA Hydrogels, and Dopamine Detection. *J. Mater. Chem. B* **2020**, *8* (6), 1277−1289.

(11) Sehgal, A.; Lalatonne, Y.; Berret, J.-F.; Morvan, M. Precipitation−Redispersion of Cerium Oxide Nanoparticles with Poly(Acrylic Acid): Toward Stable Dispersions. *Langmuir* **2005**, *21* (20), 9359−9364.

(12) Genix, A.-C.; Oberdisse, J. Nanoparticle Self-Assembly: From Interactions in Suspension to Polymer Nanocomposites. *Soft Matter* **2018**, *14* (25), 5161−5179.

(13) Mori, H.; Müller, A. H. E.; Klee, J. E. Intelligent Colloidal Hybrids via Reversible pH-Induced Complexation of Polyelectrolyte and Silica Nanoparticles. *J. Am. Chem. Soc.* **2003**, *125* (13), 3712−3713.

(14) Yu, B.; Liang, H.; Nealey, P. F.; Tirrell, M. V.; Rumyantsev, A. M.; de Pablo, J. J. Structure and Dynamics of Hybrid Colloid-Polyelectrolyte Coacervates: Insights from Molecular Simulations. *Macromolecules* **2023**, *56* (18), 7256−7270.

(15) Gaash, D.; Dewan, S.; Leshem, A. B.; Jaiswal, K. S.; Jelinek, R.; Lampel, A. Modulating the Optical Properties of Carbon Dots by Peptide Condensates. *Chem. Commun.* **2023**, *59* (82), 12298−12301.

(16) Arcudi, F.; Đorđević, L.; Rebeccani, S.; Cacioppo, M.; Zanut, A.; Valenti, G.; Paolucci, F.; Prato, M. Lighting up the Electrochemiluminescence of Carbon Dots through Pre- and Post-Synthetic Design. *Advanced Science* **2021**, *8* (13), No. 2100125.

(17) Zhou, Y.; Mintz, K. J.; Sharma, S. K.; Leblanc, R. M. Carbon Dots: Diverse Preparation, Application, and Perspective in Surface Chemistry. *Langmuir* **2019**, *35* (28), 9115−9132.

(18) Arcudi, F.; Đorđević, L. Supramolecular Chemistry of Carbon-Based Dots Offers Widespread Opportunities. *Small* **2023**, *19* (31), No. 2300906.

(19) Singh, S.; Jelinek, R. Sunlight-Activated Phase Transformation in Carbon Dot-Hydrogel Facilitates Water Purification and Optical Switching. *ACS Appl. Polym. Mater.* **2020**, *2* (7), 2810−2818.

(20) Zulfajri, M.; Sudewi, S.; Ismulyati, S.; Rasool, A.; Adlim, M.; Huang, G. G. Carbon Dot/Polymer Composites with Various Precursors and Their Sensing Applications: A Review. *Coatings* **2021**, *11*, 1100.
(21) Ren, J.; Malfatti, L.; Innocenzi, P. Citric Acid Derived Carbon Dots, the Challenge of Understanding the Synthesis-Structure Relationship. *C (Basel)* **2021**, *7* (1), 2.
(22) Jorns, M.; Pappas, D. A Review of Fluorescent Carbon Dots, Their Synthesis, Physical and Chemical Characteristics, and Applications. *Nanomaterials* **2021**, *11*, 1448.
(23) Wu, Z. L.; Liu, Z. X.; Yuan, Y. H. Carbon Dots: Materials, Synthesis, Properties and Approaches to Long-Wavelength and Multicolor Emission. *J. Mater. Chem. B* **2017**, *5*, 3794−3809.
(24) Lim, S. Y.; Shen, W.; Gao, Z. Carbon Quantum Dots and Their Applications. *Chem. Soc. Rev.* **2015**, *44*, 362−381.
(25) Supriya, B. S.; Nagaraja, P.; Byrappa, K. Hydrothermal Synthesis and Characterization of Carbon Spheres Using Citric-Acid-Catalyzed Carbonization of Starch. *e-Polym.* **2015**, *15* (3), 179−183.
(26) Vercelli, B.; Donnini, R.; Ghezzi, F.; Sansonetti, A.; Giovanella, U.; La Ferla, B. Nitrogen-Doped Carbon Quantum Dots Obtained Hydrothermally from Citric Acid and Urea: The Role of the Specific Nitrogen Centers in Their Electrochemical and Optical Responses. *Electrochim. Acta* **2021**, *387*, 138557.
(27) Lee, H.; Su, Y. C.; Tang, H. H.; Lee, Y. S.; Lee, J. Y.; Hu, C. C.; Chiu, T. C. One-Pot Hydrothermal Synthesis of Carbon Dots as Fluorescent Probes for the Determination of Mercuric and Hypochlorite Ions. *Nanomaterials* **2021**, *11* (7), 1831.
(28) Saini, B.; Singh, R. R.; Nayak, D.; Mukherjee, T. K. Biocompatible PH-Responsive Luminescent Coacervate Nanodroplets from Carbon Dots and Poly(Diallyldimethylammonium Chloride) toward Theranostic Applications. *ACS Appl. Nano Mater.* **2020**, *3* (6), 5826−5837.
(29) Saini, B.; Singh, S.; Mukherjee, T. K. Nanocatalysis under Nanoconfinement: A Metal-Free Hybrid Coacervate Nanodroplet as a Catalytic Nanoreactor for Efficient Redox and Photocatalytic Reactions. *ACS Appl. Mater. Interfaces* **2021**, *13* (43), 51117−51131.
(30) Wang, J.; Liu, G.; Leung, K. C.; Loffroy, R.; Lu, P.; Wáng, Y. X. J. Opportunities and Challenges of Fluorescent Carbon Dots in Translational Optical Imaging. *Curr. Pharm. Des* **2015**, *21*, 5401−5416.
(31) Ding, H.; Du, F.; Liu, P.; Chen, Z.; Shen, J. DNA-Carbon Dots Function as Fluorescent Vehicles for Drug Delivery. *ACS Appl. Mater. Interfaces* **2015**, *7* (12), 6889−6897.
(32) Li, S.; Su, W.; Wu, H.; Yuan, T.; Yuan, C.; Liu, J.; Deng, G.; Gao, X.; Chen, Z.; Bao, Y.; Yuan, F.; Zhou, S.; Tan, H.; Li, Y.; Li, X.; Fan, L.; Zhu, J.; Chen, A. T.; Liu, F.; Zhou, Y.; Li, M.; Zhai, X.; Zhou, J. Targeted Tumour Theranostics in Mice via Carbon Quantum Dots Structurally Mimicking Large Amino Acids. *Nat. Biomed Eng.* **2020**, *4* (7), 704−716.
(33) Gong, N.; Ma, X.; Ye, X.; Zhou, Q.; Chen, X.; Tan, X.; Yao, S.; Huo, S.; Zhang, T.; Chen, S.; Teng, X.; Hu, X.; Yu, J.; Gan, Y.; Jiang, H.; Li, J.; Liang, X.-J. Carbon-Dot-Supported Atomically Dispersed Gold as a Mitochondrial Oxidative Stress Amplifier for Cancer Treatment. *Nat. Nanotechnol* **2019**, *14* (4), 379−387.
(34) Kirbas Cilingir, E.; Seven, E. S.; Zhou, Y.; Walters, B. M.; Mintz, K. J.; Pandey, R. R.; Wikramanayake, A. H.; Chusuei, C. C.; Vanni, S.; Graham, R. M.; Leblanc, R. M. Metformin Derived Carbon Dots: Highly Biocompatible Fluorescent Nanomaterials as Mitochondrial Targeting and Blood-Brain Barrier Penetrating Biomarkers. *J. Colloid Interface Sci.* **2021**, *592*, 485−497.
(35) Qin, K.; Zhang, D.; Ding, Y.; Zheng, X.; Tan, W.; Xiang, Y.; Hua, J.; Ji, X.; Li, B.; Wei, Y. Application of Carbon Dots Synthesized from Tryptone and Yeast Extract in Bioimaging and Highly Selective Detection of P-Nitrophenol and Nickel(Ii). *Analytical Methods* **2019**, *11* (44), 5724−5729.
(36) Hoang, V. C.; Dave, K.; Gomes, V. G. Carbon Quantum Dot-Based Composites for Energy Storage and Electrocatalysis: Mechanism, Applications and Future Prospects. *Nano Energy* **2019**, *66*, No. 104093.
(37) Chen, Y.-C.; Chiang, W.-H.; Kurniawan, D.; Yeh, P.-C.; Otake, K.; Kung, C.-W. Impregnation of Graphene Quantum Dots into a Metal−Organic Framework to Render Increased Electrical Conductivity and Activity for Electrochemical Sensing. *ACS Appl. Mater. Interfaces* **2019**, *11* (38), 35319−35326.
(38) Pace, G. T.; Le, M. L.; Clément, R. J.; Segalman, R. A. A Coacervate-Based Mixed-Conducting Binder for High-Power, High-Energy Batteries. *ACS Energy Lett.* **2023**, *8* (6), 2781−2788.
(39) Lv, K.; Perriman, A. W.; Mann, S. Photocatalytic Multiphase Micro-Droplet Reactors Based on Complex Coacervation. *Chem. Commun.* **2015**, *51* (41), 8600−8602.
(40) Liu, J.; Tian, L.; Qiao, Y.; Zhou, S.; Patil, A. J.; Wang, K.; Li, M.; Mann, S. Hydrogel-Immobilized Coacervate Droplets as Modular Microreactor Assemblies. *Angew. Chem., Int. Ed.* **2020**, *59* (17), 6853−6859.
(41) Tabandeh, S.; Ateeq, T.; Leon, L. Drug Encapsulation via Peptide-Based Polyelectrolyte Complexes. *ChemBioChem.* **2024**, *25* (1), No. e202300440.
(42) Johnson, N. R.; Ambe, T.; Wang, Y. Lysine-Based Polycation:Heparin Coacervate for Controlled Protein Delivery. *Acta Biomater* **2014**, *10* (1), 40−46.
(43) Johnson, N. R.; Wang, Y. Coacervate Delivery Systems for Proteins and Small Molecule Drugs. *Expert Opin Drug Deliv* **2014**, *11* (12), 1829−1832.
(44) Saini, B.; Singh, R.; Mukhopadhyay, S.; Mukherjee, T. K. Specific Loading and in Vitro Controlled Release of a Ru-Based Hydrophobically Encapsulated Model Anticancer Drug inside Nanoassemblies toward Stimuli-Responsive Drug Delivery. *ACS Appl. Nano Mater.* **2021**, *4* (2), 2037−2051.
(45) Sing, C. E.; Perry, S. L. Recent Progress in the Science of Complex Coacervation. *Soft Matter* **2020**, *16* (12), 2885−2914.
(46) Xin, Y.; Yuan, J. Schiff's Base as a Stimuli-Responsive Linker in Polymer Chemistry. *Polym. Chem.* **2012**, *3* (11), 3045−3055.
(47) Kung, J. C.; Tseng, I. T.; Chien, C. S.; Lin, S. H.; Wang, C. C.; Shih, C. J. Microwave Assisted Synthesis of Negative-Charge Carbon Dots with Potential Antibacterial Activity against Multi-Drug Resistant Bacteria. *RSC Adv.* **2020**, *10*, 41202−41208.
(48) Rasband, W. *ImageJ*; U.S. National Institutes of Health, Bethesda, Maryland, USA, 2011.
(49) Abramoff, M.; Magalhães, P.; Ram, S. J. Image Processing with ImageJ. *Biophotonics International* **2003**, *11*, 36−42.
(50) Schneider, C. A.; Rasband, W. S.; Eliceiri, K. W. NIH Image to ImageJ: 25 Years of Image Analysis. *Nat. Methods* **2012**, *9* (7), 671−675.
(51) Li, X.; Zhang, S.; Kulinich, S. A.; Liu, Y.; Zeng, H. Engineering Surface States of Carbon Dots to Achieve Controllable Luminescence for Solid-Luminescent Composites and Sensitive Be^{2+} Detection. *Sci. Rep* **2014**, *4*, 4976.
(52) Đorđević, L.; Arcudi, F.; Cacioppo, M.; Prato, M. A Multifunctional Chemical Toolbox to Engineer Carbon Dots for Biomedical and Energy Applications. *Nature Nanotechnology* **2022**, *17*, 112−130.
(53) Ogi, T.; Aishima, K.; Permatasari, F. A.; Iskandar, F.; Tanabe, E.; Okuyama, K. Kinetics of Nitrogen-Doped Carbon Dot Formation via Hydrothermal Synthesis. *New J. Chem.* **2016**, *40* (6), 5555−5561.
(54) Wang, B.-B.; Jin, J.-C.; Xu, Z.-Q.; Jiang, Z.-W.; Li, X.; Jiang, F.-L.; Liu, Y. Single-Step Synthesis of Highly Photoluminescent Carbon Dots for Rapid Detection of Hg2+ with Excellent Sensitivity. *J. Colloid Interface Sci.* **2019**, *551*, 101−110.
(55) Deng, W. W.; Zang, C. R.; Li, Q. C.; Sun, B.; Mei, X. P.; Bai, L.; Shang, X. M.; Deng, Y.; Xiao, Y. Q.; Ghiladi, R. A.; Lorimer, G. H.; Zhang, X. J.; Wang, J. Hydrothermally Derived Green Carbon Dots from Broccoli Water Extracts: Decreased Toxicity, Enhanced Free-Radical Scavenging, and Anti-Inflammatory Performance. *ACS Biomater Sci. Eng.* **2023**, *9* (3), 1307−1319.
(56) Das, A.; Kundelev, E. V.; Vedernikova, A. A.; Cherevkov, S. A.; Danilov, D. V.; Koroleva, A. V.; Zhizhin, E. V.; Tsypkin, A. N.; Litvin,

https://doi.org/10.1021/acsmacrolett.4c00745
ACS Macro Lett. 2025, 14, 43−50

A. P.; Baranov, A. V.; Fedorov, A. V.; Ushakova, E. V.; Rogach, A. L. Revealing the Nature of Optical Activity in Carbon Dots Produced from Different Chiral Precursor Molecules. *Light Sci. Appl.* **2022**, *11* (1), 92.
(57) Sciortino, A.; Gazzetto, M.; Buscarino, G.; Popescu, R.; Schneider, R.; Giammona, G.; Gerthsen, D.; Rohwer, E. J.; Mauro, N.; Feurer, T.; Cannizzo, A.; Messina, F. Disentangling Size Effects and Spectral Inhomogeneity in Carbon Nanodots by Ultrafast Dynamical Hole-Burning. *Nanoscale* **2018**, *10* (32), 15317−15323.
(58) Kamura, Y.; Imura, K. Space-Selective Fabrication of Light-Emitting Carbon Dots in Polymer Films Using Electron-Beam-Induced Chemical Reactions. *ACS Omega* **2019**, *4* (2), 3380−3384.
(59) Seven, E. S.; Kirbas Cilingir, E.; Bartoli, M.; Zhou, Y.; Sampson, R.; Shi, W.; Peng, Z.; Ram Pandey, R.; Chusuei, C. C.; Tagliaferro, A.; Vanni, S.; Graham, R. M.; Seven, Y. B.; Leblanc, R. M. Hydrothermal vs Microwave Nanoarchitechtonics of Carbon Dots Significantly Affects the Structure, Physicochemical Properties, and Anti-Cancer Activity against a Specific Neuroblastoma Cell Line. *J. Colloid Interface Sci.* **2023**, *630*, 306−321.
(60) Liu, S.; Cui, J.; Huang, J.; Tian, B.; Jia, F.; Wang, Z. Facile One-Pot Synthesis of Highly Fluorescent Nitrogen-Doped Carbon Dots by Mild Hydrothermal Method and Their Applications in Detection of Cr(VI) Ions. *Spectrochim Acta A Mol. Biomol Spectrosc* **2019**, *206*, 65−71.
(61) Yuan, M.; Zhong, R.; Gao, H.; Li, W.; Yun, X.; Liu, J.; Zhao, X.; Zhao, G.; Zhang, F. One-Step, Green, and Economic Synthesis of Water-Soluble Photoluminescent Carbon Dots by Hydrothermal Treatment of Wheat Straw, and Their Bio-Applications in Labeling, Imaging, and Sensing. *Appl. Surf. Sci.* **2015**, *355*, 1136−1144.
(62) Karoui, H.; Seck, M. J.; Martin, N. Self-Programmed Enzyme Phase Separation and Multiphase Coacervate Droplet Organization. *Chem. Sci.* **2021**, *12* (8), 2794−2802.
(63) Zhang, Y.; Liu, S.; Yao, Y.; Chen, Y.; Zhou, S.; Yang, X.; Wang, K.; Liu, J. Invasion and Defense Interactions between Enzyme-Active Liquid Coacervate Protocells and Living Cells. *Small* **2020**, *16* (29), 2002073.
(64) Qiao, C.; Qian, L.; Peng, Q.; Yue, W. Heteropolysaccharide-Based Coacervate Microdroplets as Enzyme Carriers for Detection of Cholesterol. *ACS Appl. Polym. Mater.* **2024**, *6* (10), 5586−5592.
(65) Zhu, S.; Meng, Q.; Wang, L.; Zhang, J.; Song, Y.; Jin, H.; Zhang, K.; Sun, H.; Wang, H.; Yang, B. Highly Photoluminescent Carbon Dots for Multicolor Patterning, Sensors, and Bioimaging. *Angew. Chem., Int. Ed.* **2013**, *52* (14), 3953−3957.
(66) Li, H.; Kang, Z.; Liu, Y.; Lee, S.-T. Carbon Nanodots: Synthesis, Properties and Applications. *J. Mater. Chem.* **2012**, *22* (46), 24230−24253.
(67) Shauloff, N.; Bhattacharya, S.; Jelinek, R. Elastic Carbon Dot/Polymer Films for Fluorescent Tensile Sensing and Mechano-Optical Tuning. *Carbon N Y* **2019**, *152*, 363−371.
(68) De, B. Carbon Dots and Their Polymeric Nanocomposites. In *Nanomaterials and Polymer Nanocomposites*; Karak, N., Ed.; Elsevier, 2019; Chapter 7, pp 217−260. DOI: 10.1016/B978-0-12-814615-6.00007-2.
(69) Alshareedah, I.; Moosa, M. M.; Pham, M.; Potoyan, D. A.; Banerjee, P. R. Programmable Viscoelasticity in Protein-RNA Condensates with Disordered Sticker-Spacer Polypeptides. *Nat. Commun.* **2021**, *12* (1), 6620.
(70) Alshareedah, I.; Singh, A.; Yang, S.; Ramachandran, V.; Quinn, A.; Potoyan, D. A.; Banerjee, P. R. Determinants of Viscoelasticity and Flow Activation Energy in Biomolecular Condensates. *Sci. Adv.* **2024**, *10*, eadi6539.
(71) Alshareedah, I.; Singh, A.; Quinn, A.; Banerjee, P. R. *Determinants of Viscoelasticity and Flow Activation Energy in Biomolecular Condensates*; Alshareedah, I., Singh, A., Quinn, A., Banerjee, P. R., Eds.; Department of Physics, University at Buffalo, Buffalo, NY 14260, U.S.A., 2022.
(72) Ceballos, A. V.; Diaz A, J. A.; Preston, J. M.; Vairamon, C.; Shen, C.; Koder, R. L.; Elbaum-Garfinkle, S. Liquid to Solid Transition of Elastin Condensates. *Biophys. Comput. Biol.* **2022**, *119*, e2202240119.
(73) Park, S.; Barnes, R.; Lin, Y.; Jeon, B.-j.; Najafi, S.; Delaney, K. T.; Fredrickson, G. H.; Shea, J. E.; Hwang, D. S.; Han, S. Dehydration Entropy Drives Liquid-Liquid Phase Separation by Molecular Crowding. *Commun. Chem.* **2020**, *3* (1), 83.
(74) Soussi Hachfi, R.; Famelart, M.-H.; Rousseau, F.; Hamon, P.; Bouhallab, S. Rheological Characterization of β-Lactoglobulin/Lactoferrin Complex Coacervates. *LWT* **2022**, *163*, No. 113577.
(75) Fisher, R. S.; Elbaum-Garfinkle, S. Tunable Multiphase Dynamics of Arginine and Lysine Liquid Condensates. *Nat. Commun.* **2020**, *11* (1), 4628.
(76) Michieletto, D.; Marenda, M. Rheology and Viscoelasticity of Proteins and Nucleic Acids Condensates. *JACS Au.* **2022**, *2*, 1506−1521.
(77) Meng, X.; Perry, S. L.; Schiffman, J. D. Complex Coacervation: Chemically Stable Fibers Electrospun from Aqueous Polyelectrolyte Solutions. *ACS Macro Lett.* **2017**, *6* (5), 505−511.
(78) Sun, J.; Perry, S. L.; Schiffman, J. D. Electrospinning Nanofibers from Chitosan/Hyaluronic Acid Complex Coacervates. *Biomacromolecules* **2019**, *20* (11), 4191−4198.
(79) Sadman, K.; Delgado, D. E.; Won, Y.; Wang, Q.; Gray, K. A.; Shull, K. R. Versatile and High-Throughput Polyelectrolyte Complex Membranes via Phase Inversion. *ACS Appl. Mater. Interfaces* **2019**, *11* (17), 16018−16026.
(80) Kelly, K. D.; Schlenoff, J. B. Spin-Coated Polyelectrolyte Coacervate Films. *ACS Appl. Mater. Interfaces* **2015**, *7* (25), 13980−13986.
(81) Kurtz, I. S.; Sui, S.; Hao, X.; Huang, M.; Perry, S. L.; Schiffman, J. D. Bacteria-Resistant, Transparent, Free-Standing Films Prepared from Complex Coacervates. *ACS Appl. Bio Mater.* **2019**, *2* (9), 3926−3933.